

Graphene-ophicalcite heterogeneous composite sponge for rapid hemostasis

Bingxin Wu^a, Fanglin Du^a, Wenjing A^a, Fang Liu^b, Yichun Liu^a, Weitao Zheng^c, Guofeng Li^{a,*}, Xing Wang^{a,*}

^a State Key Laboratory of Organic-Inorganic Composites, Beijing Laboratory of Biomedical Materials, Beijing University of Chemical Technology, Beijing 100029, China

^b Department of Oncology of Integrative Chinese and Western Medicine, China-Japan Friendship Hospital, Beijing 100029, China

^c Hubei Provincial Key Laboratory of Industrial Microbiology, Sino-German Biomedical Center, National "111" Center for Cellular Regulation and Molecular Pharmaceutics, Hubei University of Technology, Wuhan 430068, Hubei Province, China

ARTICLE INFO

Keywords:

Grapheme
Ophicalcite
Heterogeneous
Composite sponge
Hemostasis

ABSTRACT

Synergistic functionalization of interface coagulation stimulation and liquid absorption capacity is the key to improve the hemostatic efficiency of hemostats. Herein, we prepared a graphene-ophicalcite (OPH) heterogeneous composite sponge (GOCS) by using the heterogeneous gradient composite strategy. The sponge took cross-linked graphene sponge (CGS) as the main skeleton, allowing the OPH to be controllably positioned on the surface of GOCS. The heterogeneous strategy gave full play to the advantages of the material. On the one hand, GOCS had excellent liquid absorption ability, which enriched blood cells and other coagulation components at the wound interface after contacting blood. On the other hand, the OPH at the interface obviously activated platelets and rapidly triggered coagulation cascade reactions, exhibiting fast response and feedback characteristics for coagulation signals. Under the synergistic effects, the blood clotting index value of GOCS was reduced to $33.87 \pm 9.97\%$, which was significantly lower than those of OPH ($46.33 \pm 16.85\%$) and CGS ($67.53 \pm 5.35\%$). Importantly, GOCS rapidly stopped bleeding within 51 s in the rat femoral artery model, suggesting its great potential in the field of hemostasis. Therefore, this study provides a new idea for the design and preparation of hemostatic materials via heterogeneous strategy.

1. Introduction

The main cause of traumatic death is the uncontrolled massive bleeding and accompanying complications [1,2]. The death rate in the battlefield is as high as 50% [3]. Therefore, using effective hemostatic materials to intervene in external bleeding is meaningful. At present, the common hemostatic materials can be divided into three categories: (1) Organic hemostatic materials, such as natural polysaccharides, thrombin, recombinant factor VIIa and fibrin [4,5]. (2) Inorganic hemostatic materials, such as kaolin, zeolite, and mesoporous silica gel [6–8]. (3) Composite hemostatic materials, such as chitosan/starch composite hemostatic sponge [7]. Cross-linked graphene sponge (CGS) is a new type of hemostatic material [9]. It achieves effective hemostasis because of its superior liquid absorption capacity. CGS can rapidly absorb plasma within milliseconds, and then enrich blood cells in the interface of wound to form primary hemostatic cell-plug, which is the premise and basis for hemostasis. However, the hemostatic mechanism

of CGS is only physical absorption, which cannot directly stimulate platelets and activate coagulation cascade. While coagulation cascade is a critical process of hemostasis, it jointly promotes the formation of fibrin and finally forms blood scab [10]. Therefore, an ideal hemostatic sponge should have the ability not only to quickly absorb plasma, enrich platelets at the interface between wound and material, but also to activate the coagulation cascade at the interface at the same time.

Interface functional differentiation could be realized by the construction of heterogeneous materials. Heterogeneous material is a new type of composite material with uneven distribution and changed composition and structure. Due to the heterogeneity of its physical and chemical properties, it has attracted great interest in many practical applications, such as biomolecular interaction, cell motion, microfluidic manufacturing and so on [11]. In recent years, heterogeneous materials have also been applied in the field of hemostasis. Huang et al [12] prepared an oxidized regenerated cellulose hemostat with gradient sodium carboxylate groups to promote rapid gelation of hemostasis.

* Corresponding authors.

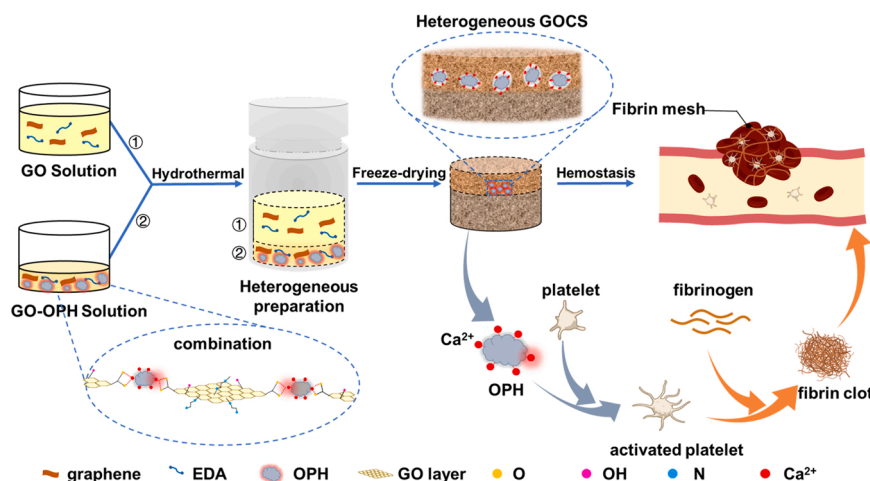
E-mail addresses: ligf@mail.buct.edu.cn (G. Li), wangxing@mail.buct.edu.cn (X. Wang).

<https://doi.org/10.1016/j.colsurfb.2022.112596>

Received 15 February 2022; Received in revised form 18 May 2022; Accepted 22 May 2022

Available online 25 May 2022

0927-7765/© 2022 Elsevier B.V. All rights reserved.



Scheme 1. Preparation flow chart of GOCS. GO sheets, OPH powders, EDA linkers are applied to prepare the heterogeneous hydrogel by a heterogeneous hydrothermal reaction. After freeze-drying and puffing, the final composite sponge can be obtained, where OPH powders can be controllably aggregated on the surface of GOCS and combine with cross-linked GO sheets stably. GOCS can activate platelets, promote fibrin clot formation and effectively stop bleeding.

Further, Ma et al [13]. developed a heterogeneous carboxymethyl chitosan (PWCS) fibers using ethanol-water exhaustion method, which led to a controllable swelling performance to achieve rapid hemostasis and antibiosis. Sui et al [14]. synthesized a Janus nanocellulose sponge with differentiated wettability surfaces to accelerate blood coagulation and prevent bacterial penetration. Mao et al [15]. prepared a modified cotton fabric with asymmetric wettability (Janus) using a simple and subtle spray-coating strategy. The hydrophilic side endowed the material rapid blood absorption and promoted hemostasis, while the excessive blood absorption could be prevented by the hydrophobic side. Therefore, the heterogeneous gradient strategy is a feasible approach to introduce multiple hemostatic functions in one material. Since the traumatic hemostasis occurs at the interface, utilizing heterogeneous composites to reinforce interface stimulation on the premise of rapid liquid absorption, mimicking the bioprocess of coagulation cascade, which will enhance the hemostatic performance of the hemostat and further expand the prospect of heterogeneous strategy.

Ophicalcite (OPH) is a kind of natural mineral medicine that mainly composes of CaCO_3 and MgCO_3 , mixing with a small amount of iron salt, zinc, copper, cobalt and acid insoluble [16]. Ca^{2+} is a universal coagulation factor and participates in the important process of coagulation cascade reaction (including endogenous/exogenous/common coagulation pathway) [17]. Besides, the increase of Ca^{2+} concentration will lead to the densification of blood vessels, stimulate and aggregate platelets, and effectively prevent blood exudation. Subsequently, prothrombin is transformed into thrombin, and fibrinogen is crosslinked to form fibrin clot. Based on this, OPH can be endowed with good hemostatic potential because of the abundant Ca^{2+} . However, with a long history, OPH is mainly used as oral Chinese medicine, and rarely used in the field of trauma hemostasis.

Herein, we fabricated a graphene-OPH heterogeneous composite sponge (GOCS) via a hydrothermal reaction using heterogeneously distributed OPH (Scheme 1). The reacted suspension of OPH and graphene oxide (GO)/ethylenediamine (EDA) was laid in the reactor, and then was slowly covered with the other suspension of GO/EDA without OPH. Ca^{2+} in OPH can stably complex with carboxyl group in GO to successfully synthesize materials. This gradient recombination strategy enriched OPH on the surface and presented a gradient distribution in the whole GOCS. As a new stimulant, the surface OPH resulted in a rapid response at the interface between wound and GOCS, so as to activate the coagulation cascade efficiently. Additionally, the inner of GOCS without OPH was equivalent to a large volume container for liquid absorption. Therefore, GOCS not only makes great use of porous structure to achieve rapid physical adsorption, but also to enhance the hemostatic interface

stimulation ability by OPH. In this way, the coordination and unity of interface stimulation ability and overall absorption are realized.

2. Experiment

2.1. Materials

A modified Hummers' method was employed to prepare the GO solution [18,19], which the concentration was 10 mg/mL. OPH was purchased from Bozhou Anbo Pharmaceutical Co., Ltd. Other reagents were purchased from Sinopharm Chemical Reagent Co., Ltd.

2.2. Preparation and characterization of the GOCS

After mixing OPH powders (5 mg) with 5 mL GO solution by high-speed agitator, 0.1 mL EDA was added and fully mixed. The obtained suspension was sealed at the bottom of the hydrothermal synthesis reactor. In the same way, only 15 mL GO and 0.3 mL EDA were mixed, and the mixed solution was slowly spread on the top of the hydrothermal synthesis reactor. The sealed reactor was heated at 96°C for 6 h to obtain hydrogel. The freeze-drying method was used to dry the hydrogel. The dried hydrogel was then extracted from Soxhlet in ethanol by 48 h, then 5 s microwave puffing was applied to obtain GOCS. Finally, the GOCS was washed with ethanol again to remove the exposed EDA.

Fourier transform infrared (FT-IR) spectra of OPH, top and bottom layer of GOCS were observed within the range of $4500\text{--}500\text{ cm}^{-1}$. X-ray photoelectron spectroscopy (XPS) was used to prove that the materials were synthesized successfully. Scanning electron microscopy (SEM, 7800) was applied to research the internal structure of GOCS. Energy-dispersive spectrometry (EDS, Hitachi S-4700) was applied to observe the element composition of GOCS. The negative potential value was assessed by zeta potential (Malvern NanoSizer ZS 2000). The difference between the weight of GOCS after fully absorbing the liquid and the initial weight could measure the absorption capacity. The high-speed camera (40 ms per frame) could record the absorption rate to observe the whole absorption process of a liquid droplet. The porosity of the sponge was determined according to the previously reported method [20].

2.3. Whole blood clotting assay in vitro

The samples (solid 1 cm^2 , powder 0.1 g) were pre-incubated at 37°C for 5 min 100 μL of anticoagulant (ACD) whole blood from SD rats was dropped onto each sample, the same position was dropped 10 μL CaCl_2

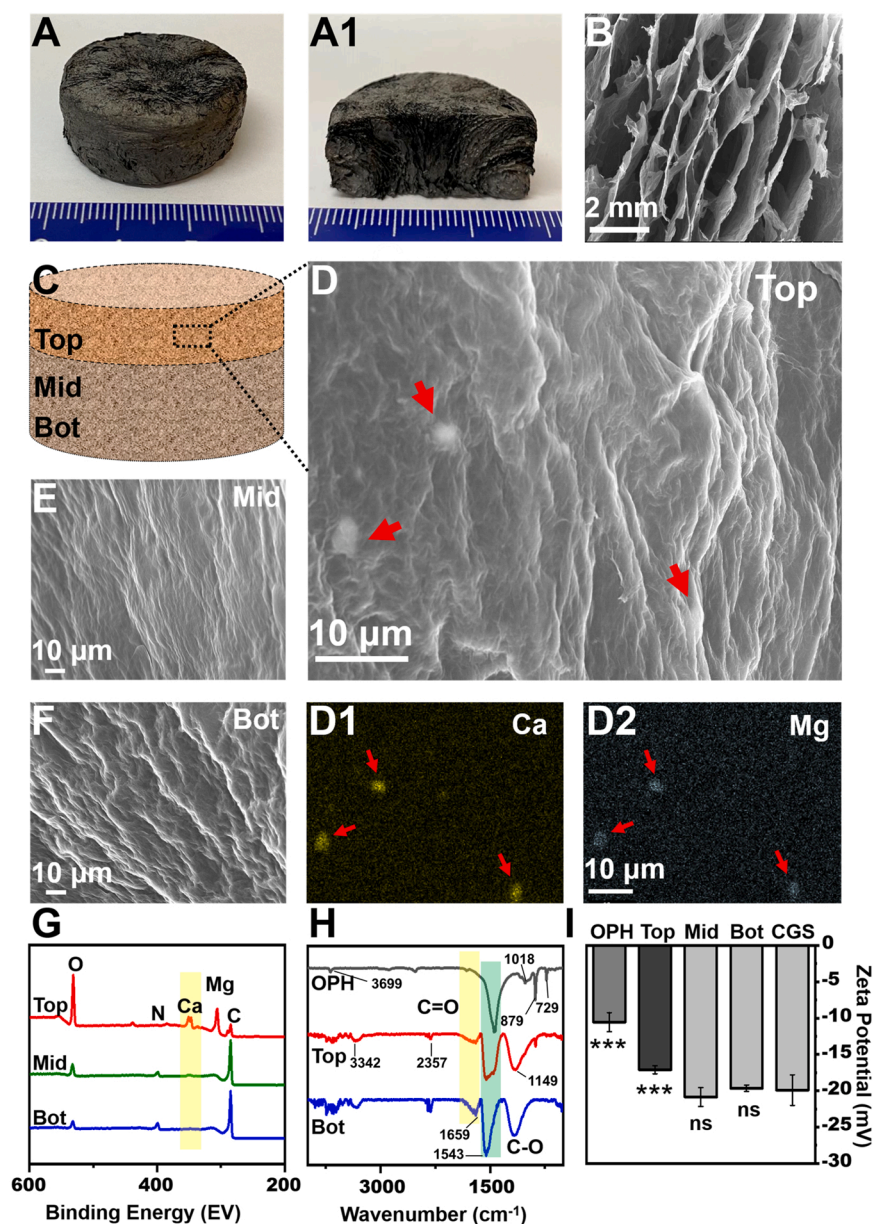


Fig. 1. (A) Photograph of GOCS. (A1) Cross section image of GOCS. (B) SEM image of the porous structure of the GOCS. (C) Brief structure diagram of GOCS. (D) SEM image of the Top of GOCS. The red arrows indicate the anchored OPH inside the GOCS. EDS mapping of (D1) Ca, (D2) Mg elements corresponding to D. SEM images of the Mid (E) and (F) the Bot of GOCS. (G) XPS spectra of the Top, Mid and Bot. (H) FTIR spectra of OPH, Top and Bot. (I) Zeta potential of the Top, Mid, Bot of GOCS, and CGS. Data values correspond to the mean \pm SD, $n = 3$; two-way ANOVA, ns represents no significant difference, $***p < 0.001$.

solution (0.2 M) subsequently. After incubating at 37 °C for 5 min, without interfering with the clotted blood, 25 mL of deionized water was added to incubate at 37 °C for 10 min. The hemoglobin absorbance of non-adherent blood clots was measured at 542 nm (donated as Abs_{sample}). The negative reference was the ACD blood in deionized water (donated as $Abs_{negative}$). The samples were subjected to three parallel experiments. The blood clotting index (BCI) of the samples were calculated by this formula: $BCI (\%) = (Abs_{sample}/Abs_{negative}) \times 100\%$.

2.4. Evaluation of the hemostatic performance

Animals were treated and cared for in accordance with the National Research Council's Guide for the care and use of laboratory animals and under the supervision and assessment by the SPF Animal Department of Clinical Institute in China–Japan Friendship Hospital (Approval no. 211001). The rat femoral artery injury model was employed to evaluate the hemostatic effect of GOCS. After anesthetizing with 10% chloral hydrate (0.5 mL/100 g), the artery was transected to cause injury and bleeding. GOCS was slightly pressed on the wound. Raising the GOCS

slightly every 10 s to observe whether the bleeding stopped. When the bleeding stopped in the gap, the blood time and loss were recorded.

2.5. Hemolysis assay in vitro

5 mL SD rats ACD blood was washed with phosphate buffered saline (PBS, pH 7.4) for three times and diluted to 50 mL in PBS to collect purified red blood cells (RBC). In order to test the hemolysis assay of GOCS and OPH, 0.2 mL of purified RBC was mixed with 0.8 mL of sample suspensions with different concentrations in PBS (15.6–1000 μg/mL). The sample was crushed by agate mortar and mixed with PBS for 2 h to prepare sample suspension. The positive and negative controls were deionized water (+ RBCs) and PBS (– RBCs), respectively. Incubating all samples in shaker at 37 °C for 3 h. Finally, after centrifuging for 5 min at 10,000 g, UV–vis spectrophotometer (UV-2450, Shimadzu) was applied to measure the hemoglobin absorbance at 540 nm. The hemolysis rate was calculated by the formula: $hemolysis\ rate (\%) = (sample\ absorption - negative\ absorption)/(positive\ absorption - negative\ absorption) \times 100\%$ [21].

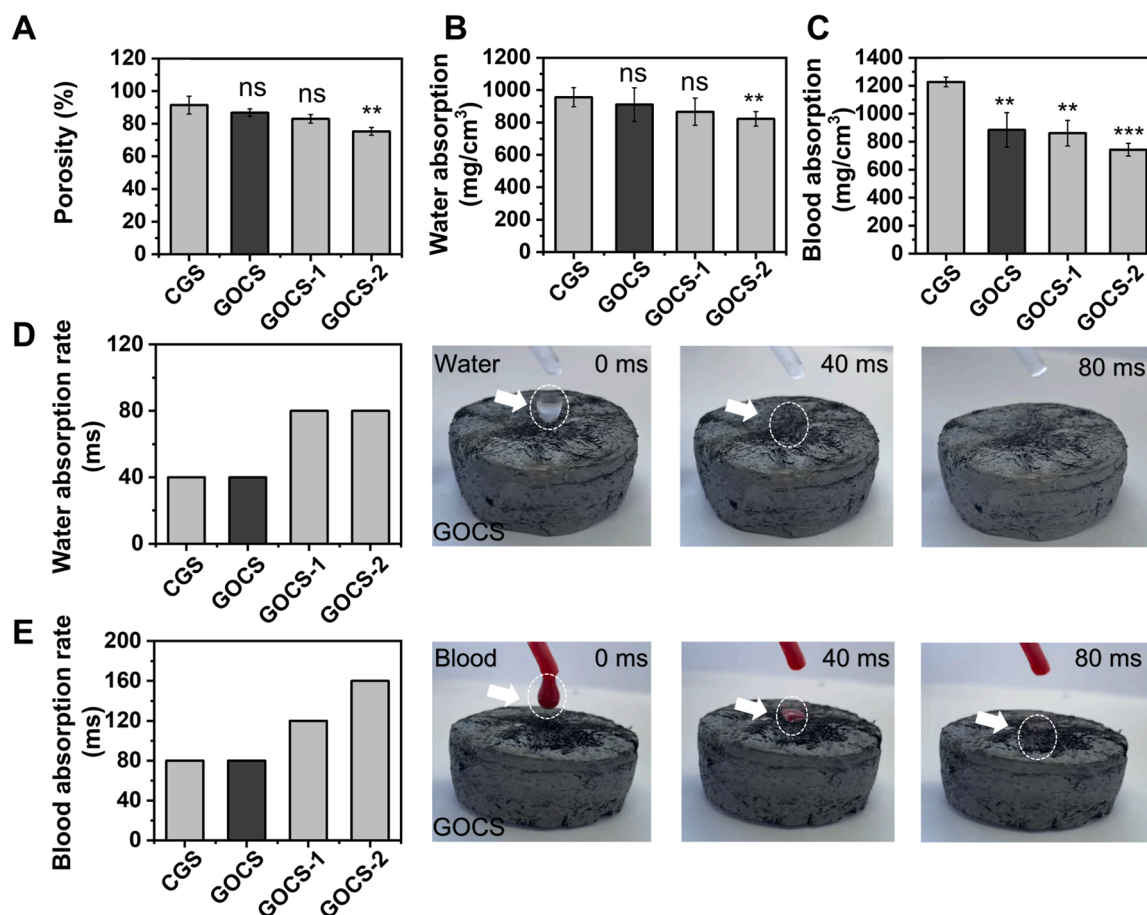


Fig. 2. (A) The porosity, (B) the water absorption amount, (C) the blood absorption amount, (D) the water absorption rate and (E) the blood absorption rate of CGS, GOCS, GOCS-1, GOCS-2. The followed photographic images specifically refer to water and blood absorption rate of GOCS. Data values correspond to the mean \pm SD, $n = 3$; two-way ANOVA, ns represents no significant difference, $**p < 0.01$, $***p < 0.001$.

2.6. Interfacial interaction between blood cells and the GOCS

To test the blood cell selective adhesion, GOCS ($1 \times 1 \text{ cm}^2$, thickness 0.25 cm) was immersed in 10 mL PBS at 37°C for 2 h. Subsequently, 0.5 mL ACD whole blood or platelet rich plasma (PRP, 1×10^5 platelets/ μL) was added and incubated with the substance for another 1 h at 37°C . After being washed with PBS for three times, the samples fixed with 2.5% glutaraldehyde at 4°C for 2 h. Finally, the samples were dehydrated with 50%, 60%, 70%, 80%, 90% and 100% of ethanol for 10 min. After freeze-drying for 12 h, and then observed by SEM [22].

In order to observe the morphology of blood cells, dropping a drop of ACD whole blood or PRP directly on the surface of GOCS (diameter 4 cm, thickness 2 cm). After incubating at 37°C for 3 min, the samples were treated according to the above method, and then observed by SEM.

2.7. APTT and PT assay

MC-2000 semiautomatic coagulation analyzer (TECO, Germany) was applied to test the prothrombin time (PT) and activated partial thromboplastin time (APTT). The fresh blood was centrifuged at 3000 rpm for 15 min at 4°C . After collecting the supernatant, the platelet poor plasma (PPP) could be obtained. The samples were incubated with PPP at 37°C for 10 min at a concentration of 0.5 mg/mL. The samples reacted with PT reagent or APTT reagent to test PT and APTT, respectively. The control group was pure PPP.

2.8. Quantitative analysis of platelet adhesion

The concentration of platelets in PBS was 2×10^8 cells/mL, then were stained with fluorescein isothiocyanate (FITC) dye. After rinsing with PBS, incubated with GOCS (0.5 mg/mL) at 37°C for 20 min, then fixed with 4% paraformaldehyde at 4°C for 2 h. The platelets were cultured onto confocal petri dish coated with fibrinogen (100 $\mu\text{g}/\text{mL}$) for 30 min at room temperature. After rinsing with PBS, the adhered platelets were observed under a confocal microscope [23].

2.9. Cytotoxicity assay

L929 mouse fibroblast cells were used to evaluate the cytotoxicity of GOCS and OPH. The number of L929 mouse fibroblast cells were adjusted to 5×10^5 cells/mL in complete medium (CM). Then, 250 $\mu\text{g}/\text{mL}$ and 62.5 $\mu\text{g}/\text{mL}$ GOCS or the OPH suspension (prepared as Section 2.5) were incubated with L929 cells. By culturing for 24 h, the cells morphology can be observed by electronic microscope.

3. Results and discussion

3.1. Material characterization

Fig. 1 A showed the macrostructure of the GOCS (3 cm diameter and 2 cm thickness). The heterogeneous sponge perfectly inherited the porous structure of CGS (Fig. 1A1). Cross-section SEM images clearly showed that there were a large number of honeycomb-like pores in GOCS (Fig. 1B). They presented an obvious bubble-like cross-linking

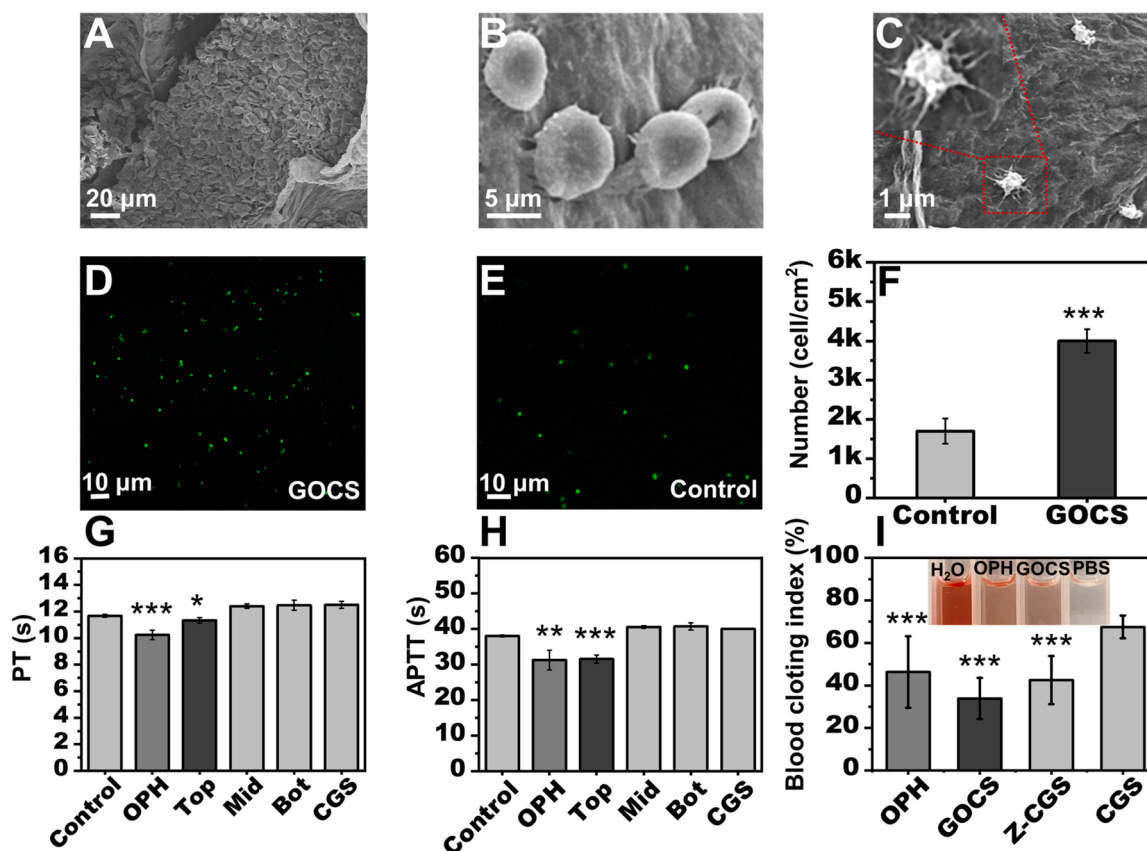


Fig. 3. (A) SEM of blood cell aggregation after direct dropping of whole blood. (B) Blood cells and (C) platelets could selectively adhere on the surface of the GOCs and change morphology. Adhesion and diffusion of platelets on immobilized fibrinogen, (D) GOCs (0.5 mg/mL), (E) Untreated platelets. (F) Statistical analysis of the number of activated platelets. (G) PT, and (H) APTT of OPH, Top, Mid, Bot, and the CGS (data values correspond to the mean \pm SD, $n = 3$; two-way ANOVA, * $p < 0.05$, ** $p < 0.01$, *** $p < 0.001$). (I) The BCI of OPH, GOCs, Z-CGS and CGS. (The lighter the color, the lower the BCI value; The darker the color, the higher the BCI value).

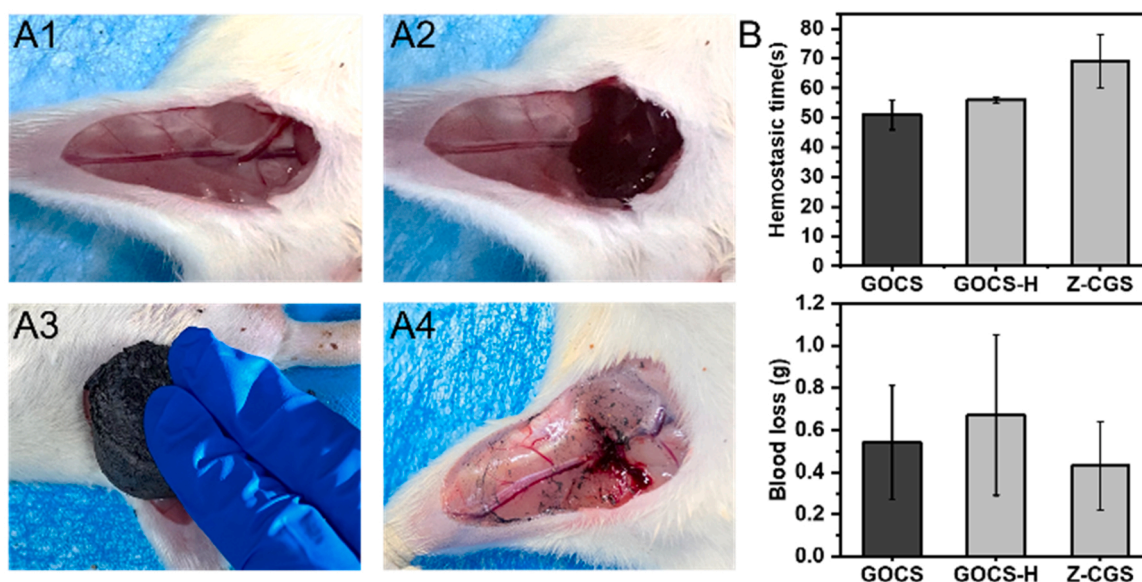
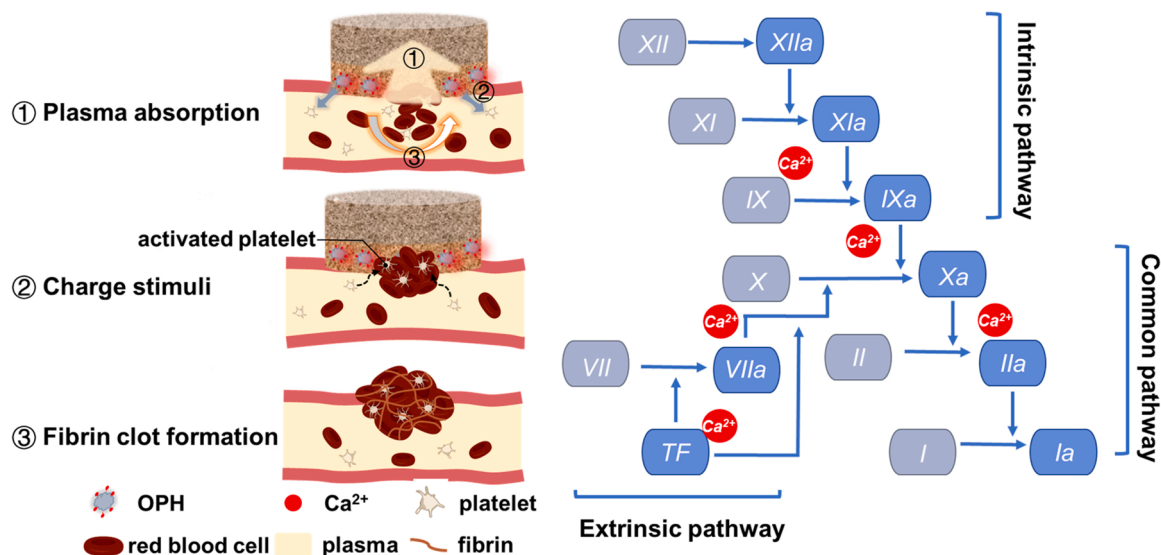


Fig. 4. (A1) Causing arterial injury. (A2) Bleeding from the wound. (A3) GOCs was employed to hemostasis. (A4) Wound after removing material after hemostasis has been completed. (B) Hemostatic time and blood loss of the GOCs in the SD rat artery injury model.

stacking state and maintained the solid overall structure of the sponge. Subsequently, we divided the heterogeneous gradient sponge into three layers (Fig. 1 C): the top layer (denoted as Top, rich in OPH), the middle

layer (denoted as Mid, containing trace OPH) and the bottom layer (denoted as Bot, excluding OPH). The secondary addition strategy of material preparation fused the interface between the Mid and the Bot,



Scheme 2. Schematic diagram of potential hemostatic synergy of GOCS. (1) absorbing of plasma quickly within the sponge, enriching blood cells on the surface of sponge, (2) stimulating platelets and clotting factors activation by the charge of OPH, and (3) forming fibrin clots and promoting blood coagulation, achieving ultrafast hemostasis.

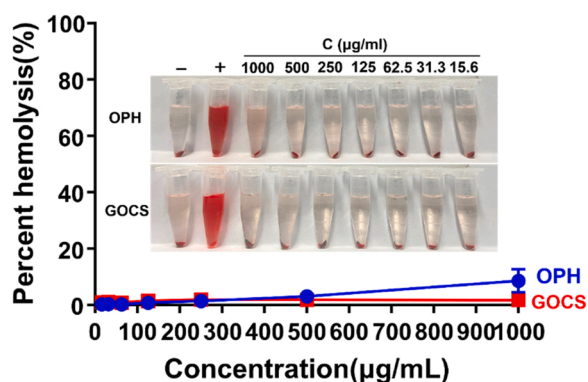


Fig. 5. Hemolysis assays for the GOCS and the OPH powders.

but the Ca^{2+} in OPH could combine with the carboxyl group at the edge of GO that enabled OPH to stably distribute in the Top phase. The OPH powders were anchored on the Top of GOCS, and the size were about 1–4 μm (Fig. 1D). EDS mapping confirmed that Ca and Mg elements in the Top of GOCS (Fig. 1D1-D2), which were the characteristic components of OPH. Conversely, the Mid (Fig. 1E) and the Bot (Fig. 1F) did not show any obvious component of OPH. Only the graphene wrinkles were observed, which is a common feature of GO [24]. This implied that the OPH was mainly distributed on the Top of GOCS. The distribution of OPH was further investigated using XPS (Fig. 2G). Ca element was detected only in the Top of GOCS, suggesting the heterogeneous distribution of OPH. Because the main component of OPH is CaCO_3 , the O element in the Top group was significantly increased compared with that in the Mid and Bot. FTIR was used to verify the interaction between Ca^{2+} in OPH and carboxyl groups in GO [25]. Compared with the FTIR spectrum of Bot group, the FTIR spectrum of the Top group exhibited that the stretch intensity of $\text{C}=\text{O}$ was decreased, the stretch intensity of carboxyl $\text{C}-\text{O}$ was increased (Fig. 2H). Besides, their peak positions were also shifted to lower wavenumbers. This was usually interpreted as evidence of coordination between carboxylic acids and divalent metal ions (Ca^{2+} , Mg^{2+}) [26,27], indicating the cross-linking between OPH and GO sheets. Further, for OPH spectrum, 3699 cm^{-1} belonged to $\text{O}-\text{H}$ telescopic vibration; 1018 cm^{-1} was SiO_4^{2-} stretching vibration absorption peak; 879 cm^{-1} and 729 cm^{-1} were CO_3^{2-} vibration absorption

peaks. In the spectra of Top and Bot, the strong absorption at about 3342 cm^{-1} could be associated with $\text{N}-\text{H}$; The absorption peak of 2357 cm^{-1} might be caused by CO_2 ; 1149 cm^{-1} was associated with the epoxy. These changes of functional groups confirmed that GOCS was cross-linked successfully. Taken together, the OPH was stably anchored on the Top of GOCS, and the graphene-OPH heterogeneous composite sponge was successfully prepared. The electronegativity of materials is important for promoting coagulation. The zeta potential of OPH was tested to be $-10.5 \pm 3.1\text{ mV}$ (Fig. 2I). After compositing, the zeta potential of the Top of GOCS decreased to $-17.1 \pm 5.6\text{ mV}$; while that of the Mid and Bot of GOCS were $-20.87 \pm 1.31\text{ mV}$ and $-19.65 \pm 0.45\text{ mV}$, respectively, which were no significant difference with that of CGS ($-19.9 \pm 2.1\text{ mV}$, cited from the reference[28]). This means that the stimulating effect of composite sponge GOCS on blood cells might be stronger than the single powder. GOCS would accelerate blood coagulation to a great extent.

The porous structure endowed GOCS with good liquid absorbability [29]. Fig. 2A showed that the porosity between GOCS (the addition amount of OPH was 0.5 mg/mL , $86.79 \pm 2.25\%$) and GOCS-1 (the addition amount of OPH was 1 mg/mL , $82.97 \pm 2.65\%$) were similar with that of CGS ($91.43 \pm 5.43\%$), showing no significant difference. While when the addition amount of OPH increased to 2 mg/mL , the porosity of the obtained GOCS-2 ($75.32 \pm 2.39\%$) decreased significantly due to the blockage of pores and the restriction of liquid flow by excessive OPH powders. For the liquid absorption capacity (Fig. 2B), the water absorption of GOCS ($910.36 \pm 103.68\text{ mg/cm}^3$) and GOCS-1 ($865.95 \pm 83.45\text{ mg/cm}^3$) were considerable with that of CGS ($955.4 \pm 59.0\text{ mg/cm}^3$, cited from the reference[30]). The water absorption of GOCS-2 decreased significantly ($821.83 \pm 45.0\text{ mg/cm}^3$), which was consistent with the porosity results. Interestingly, the blood absorption amount of GOCS decreased significantly ($883.79 \pm 122.96\text{ mg/cm}^3$) compared with that of CGS ($1226.7 \pm 35.4\text{ mg/cm}^3$, cited from the reference[30]). This was due to the fact that the surface OPH powders promoted blood coagulation, which indicated the enable of hemostatic stimulation of GOCS (Fig. 2C). Additionally, the water and blood absorption rate further illustrated the ultrafast liquid absorption capacity of GOCS. Fig. 2D and E showed that GOCS can completely absorb a drop of water within 40 ms, and that of blood was about 80 ms. The time to absorb a drop of water and blood of GOCS-1 (80 ms, 120 ms) and GOCS-2 (80 ms, 160 ms) increased due to the excessive OPH on the surface. Considering that hemostasis occurs at the interface, the

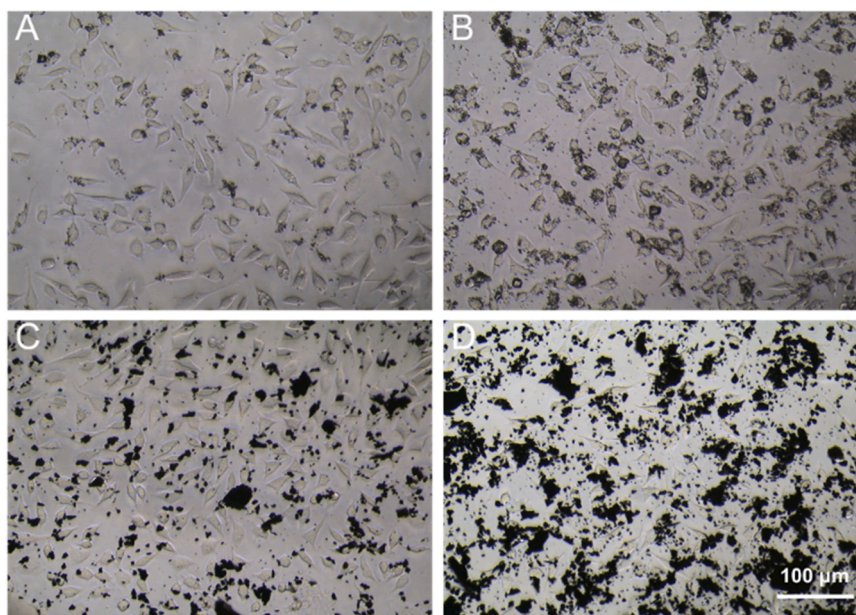


Fig. 6. Micrographs of L929 cells treated with (A) 62.5 µg/mL OPH, (B) 250 µg/mL OPH, (C) 62.5 µg/mL GOCS and (D) 250 µg/mL GOCS.

absorption rate at the interface is important. Therefore, according to the above experimental results, the GOCS with 0.5 mg/mL OPH was selected. While giving full play to the rapid liquid absorption capacity, it not only saved the cost by reducing the amount of OPH, but also effectively avoided the consequences of pore blockage caused by excessive addition.

3.2. Hemostatic performance *in vitro*

In order to clarify the hemostatic mechanism of GOCS, the morphology of blood cells and platelets on the surface of GOCS was studied [31]. As shown in Fig. 3 A, when a drop of ACD whole blood was directly dropped on the surface of GOCS, GOCS exhibited ultrafast liquid absorption. A large number of blood cells gathered on the surface and formed a blood cell layer. It was the key to the formation of blood scab. The selective adhesion of blood cells was further studied by co-incubation of GOCS (here GOCS refers to the Top of GOCS) and ACD whole blood in PBS solution. As shown in Fig. 3B, after co-incubation, the blood cells tightly adhered to GOCS. Additionally, the morphology of platelets on GOCS surface also changed obviously. The platelets extended out of spiny pseudopodia, showing an activation state (Fig. 3 C). This implied that the interface OPH reinforced the stimulation capacity, which drove GOCS to activate platelets and enhance their aggregation. Finally, the activated platelets can accelerate the production of surface thrombin. The resulting thrombin in turn triggered the conversion of fibrinogen into a stable fibrin clot [32].

In order to highlight the hemostatic stimulation effect of GOCS, the quantitative analysis of the activated platelets was further studied by a specific adhesion assay. The Bot of GOCS was used as the control group (Fig. 3D). First, platelets were pretreated with the powder of the Top of GOCS (0.5 mg/mL), and then the pretreated platelets were cultured on a confocal dish coated with fibrinogen. The platelets in an activated state could be quantitative because they would specify bind with fibrinogen (Fig. 3E). As shown in Fig. 3 F, the number of platelets adhered to the Top was high. It could reach up to 4001 cell/cm³, which was 2.3 times higher than that of the Bot (Fig. 3 F). The above results indicated that the gradient composite strategy endowed the Top of GOCS the ability to effectively stimulate platelets. One explanation was that the OPH in the Top of GOCS contained abundant Ca²⁺, which plays a widespread role in the coagulation cascade, including promoting the conversion of prothrombin to thrombin, the cross-linking of fibrin monomers and other

important steps in the coagulation cascade [17].

In order to explore the effect of GOCS on coagulation cascade, we analyzed PT and APTT in different layers of GOCS. PT and APTT perform different functions in hemostasis analysis [33]. PT is the time required to form fibrin clot after adding tissue thromboplastin, and it is an important index to prove the process of exogenous coagulation cascade. APTT is the time required to form fibrin clot after adding some thromboplastin reagent and CaCl₂, which can be used to detect endogenous coagulation cascade [17,34]. As shown in the Fig. 3 G and 3 H, the PT and APTT of OPH were significantly reduced to 10.23 ± 0.35 s and 31.3 ± 2.76 s compared with those of pure PPP (11.67 ± 0.12 s and 38.03 ± 0.25 s). When OPH was gradient embedded into GOCS, the PT and APTT of the Top group decreased to 11.33 ± 0.21 s and 31.53 ± 1.12 s. These results demonstrated that the Top of GOCS could accelerate blood coagulation by activating not only the external pathway of coagulation cascade, but also the internal pathway of coagulation cascade. This was consistent with the previously mentioned view that the role of Ca²⁺ in the coagulation cascade was ubiquitous. This gradient difference suggested that coagulation cascade was triggered mainly at the interface, which was in favor of rapid response of the coagulation process.

BCI assay was further used to investigate the *in vitro* hemostatic performance of GOCS. BCI and the hemostatic ability of the sample was reflected according to the absorbance value of hemoglobin [35]. As shown in Fig. 3I, compared with OPH (46.33 ± 16.85%) and CGS (67.53 ± 5.35%), GOCS (here GOCS refers to the Top of GOCS) significantly reduced the BCI value to 33.87 ± 9.97%, and showed the best coagulation performance. When OPH was gradient embedded, the obtained GOCS showed better coagulation performance than OPH. This result was mainly due to the synergistic effect of hemostatic stimulation of OPH and physical absorption of GOCS. Firstly, GOCS rapidly absorbed plasma and enriched components such as blood cells, platelets and coagulation factors on the surface of the material. Then, OPH on the surface of GOCS contacted and stimulated platelets activation, so as to activate the coagulation cascade system and accelerate coagulation. This was also consistent with our above research results. Compared with other materials (Z-CGS, 42.53 ± 11.3%, cited from the reference [36]), gradient composite GOCS also showed lower BCI and stronger coagulation ability, which was attributed to the fact that the gradient embedded OPH participated in the important stage of coagulation to achieve rapid hemostasis. This was consistent with the results of PT and APTT.

3.3. Hemostatic performance in vivo

The *in vivo* hemostatic performance of GOCS was assessed by a SD rats arterial injury model. First, the skin tissue and fascia were removed to expose the femoral artery of the rats (Fig. 4A1). Traumatic bleeding caused by the artery injury (Fig. 4A2). GOCS was covered on the wound, and pressure applied slightly to ensure that the Top of GOCS was in full contact with bleeding area (Fig. 4A3). After hemostasis, the GOCS was removed (Fig. 4A4). In this experiment, GOCS in direct contact with the wound, plasma was quickly absorbed into the GOCS. Then, the blood cells and platelets were accumulated at the interface between GOCS and the wound. The accumulated blood cells and platelets were further stimulated by the OPH in the Top of GOCS to accelerate the coagulation. Under this hemostatic cascade process, the wound stopped bleeding in about 51 ± 5 s (Fig. 4B). The hemostatic time was significantly shorter than that of zeolite-graphene composite sponge (Z-CGS, 69 ± 9 s, cited from the reference[36]). Moreover, the homogeneous graphene-OPH composite sponge (GOCS-H) was also used as the control group, which stopped bleeding with a slight longer time, 56 ± 1 s. In addition, the blood loss of GOCS was 0.54 ± 0.27 g (Fig. 4B), which was bounded by GOCS-H (0.67 ± 0.38 g) and Z-CGS (0.43 ± 0.21 g, cited from the reference[36]). Compared with GOCS-H, the hemostasis time of GOCS was slightly shorter and the blood loss was reduced. This illustrated that the heterogeneous strategy enabled GOCS retain the characteristics of rapid liquid absorption to adsorb the plasma at the interface. Then, the OPH located controllably on the surface of the material can obtain a rapid response and activate the platelets and coagulation cascades at the hemostatic interface. Secondly, due to the aggregation of OPH at the interface, when platelets and coagulation factors were activated, they can have a fast feedback path, so that the coagulation signal can be transmitted to the hemostatic interface faster. Finally, blood scab was formed at the interface to achieve the purpose of hemostasis. In addition, the amount of OPH in GOCS-H was 4 times than that in GOCS. The heterogeneous strategy effectively reduced the amount of OPH. It not only saved the cost, but also avoided the risk of excessive powders. Therefore, GOCS composite sponge can be used as an excellent hemostatic material for traumatic bleeding.

GOCS has been proved to be an effective hemostatic material. In our view, this was mainly due to two reasons. On the one hand, GOCS was a heterogeneous sponge that contained OPH mainly in the Top layer, while its Mid and Bot layers were the pure CGS. The construction of GOCS was based on the coagulation cascade process. The heterogeneous strategy distributed the hemostatic stimulation component, OPH, more concentrated in the Top layer. The structure of the Mid and Bot could be considered as an infinite absorption space, which greatly improved the hemostatic efficiency. In addition, OPH and GO had good charge matching. The edge of GO contained carboxyl groups, which could complex with the Ca^{2+} in OPH. Therefore, OPH powders were tightly combined in GO sheet to prevent their leakage from GOCS. This stable composite structure ensured the interface stimulation and biological safety. On the other hand, the Ca^{2+} in OPH made outstanding contributions in the field of hemostasis. Ca^{2+} as a coagulation factor plays a universal role in the coagulation cascade, including the conversion of prothrombin to thrombin, fibrin monomer crosslinking and other important steps in the coagulation cascade [37]. It includes intrinsic/extrinsic/common coagulation pathway. With the participation of Ca^{2+} , platelets secrete hemostatic media [38]. In addition, extracellular Ca^{2+} is necessary for platelet adhesion and clot contraction, which is the final stage of platelet aggregation [39]. Therefore, we believe that GOCS can achieve hemostasis through rapid absorption and hemostatic stimulation. The hemostatic mechanism of GOCS was illustrated in Scheme 2. Firstly, GOCS quickly absorbed plasma and enriched blood cells and platelets on the surface to temporarily form an initial clotting plug. Next, the accumulated blood cells and platelets contacted with the OPH in the Top layer of GOCS. The activated platelets triggered coagulation cascade process. Finally, fibrin clots formed, which blocked the wound until the

vascular tissue was repaired. Therefore, the heterogeneous composite sponge GOCS was a promising new hemostatic material, which could stop bleeding in a rapid response of ultra-fast absorption and immediate interface stimulations.

3.4. Biocompatibility assays

In vitro hemolysis test was used to evaluate the biological safety of the materials [40]. The hemolysis of the low dose of OPH (less than $500 \mu\text{g/mL}$) was the same as that of the PBS control group. When the dose increased to $1000 \mu\text{g/mL}$, slight hemolysis occurred (8.66%). On the contrary, RBCs treated with the same dose of GOCS did not show hemolysis. Only about 1.83% hemolysis was found when the dose of GOCS reached $1000 \mu\text{g/mL}$, suggesting its excellent blood compatibility (Fig. 5).

Additionally, L929 cells were selected to evaluate the cytotoxicity of OPH and GOCS [41]. When L929 cells were incubated with low dose of OPH powder ($62.5 \mu\text{g/mL}$), the cells remained in normal spindle shape with clear outline (Fig. 6A). When the dose increased to $250 \mu\text{g/mL}$, a small part of L929 cells became oval morphologies (Fig. 6B). When the cells were cultured with the same dose of GOCS, there was no obvious change in cell morphology (Fig. 6C, D). These results showed that GOCS is a safe and risk-free new generation hemostatic material.

4. Conclusions

In this paper, a novel composite hemostatic sponge (GOCS) was developed by using heterogeneous gradient strategy, and OPH was applied to the field of trauma hemostatic materials for the first time. The heterogeneous strategy enabled GOCS have the characteristics of rapid interface response. At the same time, the surface stimulator OPH can quickly feedback the coagulation signal and directly activate the endogenous and exogenous coagulation pathways. Under the synergistic effect of coagulation stimulation and physical absorption, GOCS can effectively accelerate the hemostasis process and achieve hemostasis in 51 s in rat femoral artery model. In addition, hemolysis evaluation and *in vitro* cytotoxicity evaluation emphasized that GOCS had good biocompatibility. Therefore, GOCS is a promising new hemostatic material. The heterogeneous construction strategy provides a new perspective for the development of hemostatic materials and broadens the development space in the field of hemostasis.

CRedit authorship contribution statement

Bingxin Wu: Designing and performing the experimental work, Investigation, Software, Formal analysis, Data Curation, Writing – original draft. **Fanglin Du, Wenjing A:** Helping with the material construction and *in vivo* assessments experiment. **Fang Liu, Yichun Liu:** Providing animal experiment guidance. **Weitao Zheng:** Instrument operation guidance. **Guofeng Li:** Conceiving the project, Conceptualization, Funding acquisition, Methodology, Writing – review & editing, Validation, Visualization. **Xing Wang:** Conceiving the project, Conceptualization, Methodology, Writing – review & editing, Validation, Visualization.

Declaration of Competing Interest

The authors declare that they have no known competing financial interests or personal relationships that could have appeared to influence the work reported in this paper.

Acknowledgments

G. Li thanks the National Natural Science Foundation of China (22005020) for the financial support.

References

- [1] M.A. Boerman, E. Roozen, M.J. Sanchez-Fernandez, A.R. Keerweer, R.P.F. Lanao, J. Bender, R. Hoogenboom, S.C. Leeuwenburgh, J.A. Jansen, H. Van Goor, J.C. M. Van Hest, Next generation hemostatic materials based on NHS-ester functionalized poly(2-oxazoline)s, *Biomacromolecules* 18 (8) (2017) 2529–2538.
- [2] Y. Bu, L. Zhang, J. Liu, L. Zhang, T. Li, H. Shen, X. Wang, F. Yang, P. Tang, D. Wu, Synthesis and properties of hemostatic and bacteria-responsive in situ hydrogels for emergency treatment in critical situations, *ACS Appl. Mater. Interfaces* 8 (20) (2016) 12674–12683.
- [3] X. Yang, W. Liu, N. Li, M. Wang, N. Liang, I. Ullah, A.L. Neve, Y. Feng, H. Chen, C. Shi, Design and development of polysaccharide hemostatic materials and their hemostatic mechanism, *Biomater. Sci.* 5 (12) (2017) 2357–2368.
- [4] D.A. Hickman, C.L. Pawlowski, U.D.S. Sekhon, J. Marks, A. Sen Gupta, Biomaterials and advanced technologies for hemostatic management of bleeding, *Adv. Mater.* 30 (4) (2018) 1700859.
- [5] F. Du, B. Wu, J. Liu, C. Xu, G. Li, X. Wang, Research progress of graphene-based hemostatic sponges, *Chem. J. Chin. Univ. Chin.* 42 (4) (2021) 1177–1187.
- [6] S. Pourshahrestani, E. Zeimaran, I. Djordjevic, N.A. Kadri, M.R. Towler, Inorganic hemostats: the state-of-the-art and recent advances, *Mater. Sci. Eng. C* 58 (2016) 1255–1268.
- [7] Y. Chen, L. Wu, P. Li, X. Hao, X. Yang, G. Xi, W. Liu, Y. Feng, H. He, C. Shi, Polysaccharide based hemostatic strategy for ultrarapid hemostasis, *Macromol. Biosci.* 20 (4) (2020) 1900370.
- [8] X. Wang, Q. Liu, J. Sui, S. Ramakrishna, M. Yu, Y. Zhou, X. Jiang, Y. Long, Recent advances in hemostasis at the nanoscale, *Adv. Healthcare Mater.* 8 (23) (2019) 1900823.
- [9] K. Quan, G. Li, D. Luan, Q. Yuan, L. Tao, X. Wang, Black hemostatic sponge based on facile prepared cross-linked graphene, *Colloids Surf., B* 132 (2015) 27–33.
- [10] A.M. Behrens, M.J. Sikorski, P. Kofinas, Hemostatic strategies for traumatic and surgical bleeding, *J. Biomed. Mater. Res., Part A* 102 (11) (2014) 4182–4194.
- [11] X. Yu, Z. Wang, Y. Jiang, X. Zhang, Surface gradient material: From superhydrophobicity to superhydrophilicity, *Langmuir* 22 (10) (2006) 4483–4486.
- [12] Y. Wu, J. He, W. Cheng, H. Gu, Z. Guo, S. Gao, Y. Huang, Oxidized regenerated cellulose-based hemostat with microscopically gradient structure, *Carbohydr. Polym.* 88 (3) (2012) 1023–1032.
- [13] S. Liu, Y. Yu, S. Jiang, J. Li, S. Wang, S. Chen, J. Ma, Biocompatible gradient chitosan fibers with controllable swelling and antibacterial properties, *Fibers Polym.* 22 (7) (2021) 1–9.
- [14] H. Cheng, D. Xiao, Y. Tang, B. Wang, X. Feng, M. Lu, G.J. Vancso, X. Sui, Sponges with Janus character from nanocellulose: Preparation and applications in the treatment of hemorrhagic wounds, *Adv. Healthcare Mater.* 9 (17) (2020) 1901796.
- [15] Y. Wang, D. Xiao, Y. Zhong, L. Zhang, Z. Chen, X. Sui, B. Wang, X. Feng, H. Xu, Z. Mao, Facile fabrication of carboxymethyl chitosan/paraffin coated carboxymethylated cotton fabric with asymmetric wettability for hemostatic wound dressing, *Cellulose* 27 (6) (2020) 3443–3453.
- [16] C. Mavrogenatos, A. Magganis, M. Kati, M. Broecker, P. Voudouris, Ophicalcites from the Upper Tectonic Unit on Tinos, Cyclades, Greece: mineralogical, geochemical and isotope evidence for their origin and evolution, *Int. J. Earth Sci.* 110 (3) (2021) 809–832.
- [17] J. Zhu, Y. Sun, W. Sun, Z. Meng, Q. Shi, X. Zhu, H. Gan, R. Gu, Z. Wu, G. Dou, Calcium ion-exchange cross-linked porous starch microparticles with improved hemostatic properties, *Int. J. Biol. Macromol.* 134 (2019) 435–444.
- [18] W.S. Hummers Jr, R.E. Offeman, Preparation of graphitic oxide, *J. Am. Chem. Soc.* 80 (6) (1958), 1339–1339.
- [19] Y. Shi, M. Liu, K. Wang, F. Deng, Q. Wan, Q. Huang, L. Fu, X. Zhang, Y. Wei, Bioinspired preparation of thermo-responsive graphene oxide nanocomposites in an aqueous solution, *Polym. Chem.* 6 (32) (2015) 5876–5883.
- [20] X. Yang, W. Liu, G. Xi, M. Wang, B. Liang, Y. Shi, Y. Feng, X. Ren, C. Shi, Fabricating antimicrobial peptide-immobilized starch sponges for hemorrhage control and antibacterial treatment, *Carbohydr. Polym.* 222 (2019), 115012.
- [21] K. Liao, Y. Lin, C.W. Macosko, C.L. Haynes, Cytotoxicity of graphene oxide and graphene in human erythrocytes and skin fibroblasts, *ACS Appl. Mater. Interfaces* 3 (7) (2011) 2607–2615.
- [22] R. Gu, W. Sun, H. Zhou, Z. Wu, Z. Meng, X. Zhu, Q. Tang, J. Dong, G. Dou, The performance of a fly-larva shell-derived chitosan sponge as an absorbable surgical hemostatic agent, *Biomaterials* 31 (6) (2010) 1270–1277.
- [23] S.K. Singh, M.K. Singh, M.K. Nayak, S. Kumari, S. Shrivastava, J.J. Grácio, D. Dash, Thrombus inducing property of atomically thin graphene oxide sheets, *ACS nano* 5 (6) (2011) 4987–4996.
- [24] S. Mo, L. Peng, C. Yuan, C. Zhao, W. Tang, C. Ma, J. Shen, W. Yang, Y. Yu, Y. Min, Enhanced properties of poly (vinyl alcohol) composite films with functionalized graphene, *RSC Adv.* 5 (118) (2015) 97738–97745.
- [25] S. Park, K.-S. Lee, G. Bozoklu, W. Cai, S.T. Nguyen, R.S. Ruoff, Graphene oxide papers modified by divalent ions-Enhancing mechanical properties via chemical cross-linking, *ACS nano* 2 (3) (2008) 572–578.
- [26] K. Nakamoto (Ed.), *Infrared and Raman spectra of inorganic and coordination compounds*, 4th ed., John Wiley & Sons, New York, 1986, pp. 231–233.
- [27] L. Bai, D. Zhao, Y. Xu, J. Zhang, Y. Gao, L. Zhao, J. Tang, Inductive heating property of graphene oxide-Fe₃O₄ nanoparticles hybrid in an AC magnetic field for localized hyperthermia, *Mater. Lett.* 68 (2012) 399–401.
- [28] Y. Liang, C. Xu, G. Li, T. Liu, J. Liang, X. Wang, Graphene-kaolin composite sponge for rapid and riskless hemostasis, *Colloids Surf., B* 169 (2018) 168–175.
- [29] L. Wang, Y. Zhong, C. Qian, D. Yang, J. Nie, G. Ma, A natural polymer-based porous sponge with capillary-mimicking microchannels for rapid hemostasis, *Acta Biomater.* 114 (2020) 193–205.
- [30] G. Li, K. Quan, Y. Liang, T. Li, Q. Yuan, L. Tao, Q. Xie, X. Wang, Graphene-montmorillonite composite sponge for safe and effective hemostasis, *ACS Appl. Mater. Interfaces* 8 (51) (2016) 35071–35080.
- [31] K. Quan, G. Li, L. Tao, Q. Xie, Q. Yuan, X. Wang, Diaminopropionic acid reinforced graphene sponge and its use for hemostasis, *ACS Appl. Mater. Interfaces* 8 (12) (2016) 7666–7673.
- [32] T. Yan, F. Cheng, X. Wei, Y. Huang, J. He, Biodegradable collagen sponge reinforced with chitosan/calcium pyrophosphate nanoflowers for rapid hemostasis, *Carbohydr. Polym.* 170 (2017) 271–280.
- [33] Y. Huang, L. Feng, Y. Zhang, L. He, C. Wang, J. Xu, J. Wu, T.B. Kirk, R. Guo, W. Xue, Hemostasis mechanism and applications of N-alkylated chitosan sponge, *Polym. Adv. Technol.* 28 (9) (2017) 1107–1114.
- [34] M.S. Adhyapak, M.S. Kachole, Investigation of adverse effects of interactions between herbal drugs and natural blood clotting mechanism, *J. Thromb. Thrombolysis* 41 (4) (2016) 644–647.
- [35] S. Cao, Y. Yang, S. Zhang, K. Liu, J. Chen, Multifunctional dopamine modification of green antibacterial hemostatic sponge, *Mater. Sci. Eng. C* 127 (2021), 112227.
- [36] Y. Liang, C. Xu, F. Liu, S. Du, G. Li, X. Wang, Eliminating heat injury of zeolite in hemostasis via thermal conductivity of graphene sponge, *ACS Appl. Mater. Interfaces* 11 (27) (2019) 23848–23857.
- [37] M.N. Sundaram, U. Mony, P.K. Varma, J. Rangasamy, Vasoconstrictor and coagulation activator entrapped chitosan based composite hydrogel for rapid bleeding control, *Carbohydr. Polym.* 258 (2021), 117634.
- [38] A.K. Taskin, M. Yasar, I. Ozaydin, B. Kaya, O. Bat, S. Ankarali, U. Yildirim, M. Aydin, The hemostatic effect of calcium alginate in experimental splenic injury model, *Ulusal Travma Ve Acil Cerrahi Derg. Turk. J. Trauma Emerg. Surg.* 19 (3) (2013) 195–199.
- [39] Y. Wang, P. Zhou, D. Xiao, Y. Liu, Y. Zhong, B. Wang, L. Zhang, Z. Chen, X. Sui, X. Feng, H. Xu, Z. Mao, Calcium functionalized carboxymethylated cotton fabric for hemostatic wound dressing, *Cellulose* 27 (17) (2020) 10139–10149.
- [40] A. Sasidharan, L.S. Panchakarla, A.R. Sadanandan, A. Ashokan, P. Chandran, C. M. Girish, D. Menon, S.V. Nair, C. Rao, M. Koyakutty, Hemocompatibility and macrophage response of pristine and functionalized graphene, *Small* 8 (8) (2012) 1251–1263.
- [41] P.D. Bowman, X. Wang, M.A. Meledeo, M.A. Dubick, B.S. Kheirabadi, Toxicity of aluminum silicates used in hemostatic dressings toward human umbilical veins endothelial cells, HeLa cells, and RAW267.4 mouse macrophages, *J. Trauma Inj. Infect. Crit. Care* 71 (3) (2011) 727–732.